

Self-Supervised Vessel Segmentation via Adversarial Learning

Yuxin Ma¹, Yang Hua², Hanming Deng¹, Tao Song¹, Hao Wang³, Zhengui Xue¹,
 Heng Cao⁴, Ruhui Ma¹, Haibing Guan¹

¹Shanghai Jiao Tong University

³Louisiana State University

²Queen's University Belfast

⁴Shanghai General Hospital

Abstract

Vessel segmentation is critically essential for diagnosing a series of diseases, e.g., coronary artery disease and retinal disease. However, annotating vessel segmentation maps of medical images is notoriously challenging due to the tiny and complex vessel structures, leading to insufficient available annotated datasets for existing supervised methods and domain adaptation methods. The subtle structures and confusing background of medical images further suppress the efficacy of unsupervised methods. In this paper, we propose a self-supervised vessel segmentation method via adversarial learning. Our method learns vessel representations by training an attention-guided generator and a segmentation generator to simultaneously synthesize fake vessels and segment vessels out of coronary angiograms. To support the research, we also build the first X-ray angiography coronary vessel segmentation dataset, named XCAD. We evaluate our method extensively on multiple vessel segmentation datasets, including the XCAD dataset, the DRIVE dataset, and the STARE dataset. The experimental results show our method suppresses unsupervised methods significantly and achieves competitive performance compared with supervised methods and traditional methods.

1. Introduction

As the most common heart disease, coronary artery disease is one of the leading causes of death in the world. Atherosclerosis in the coronary artery hinders blood from normally flowing into the heart, eventually leading to a heart attack. Among various imaging modalities, X-ray angiography is taken as a gold standard for coronary artery disease diagnosis. As X-ray angiography can quickly display small vessel branches with a high resolution, it has been widely utilized in medical diagnosis for determining the presence, location, degree, and scope of coronary artery stenosis. It is crucial but challenging to accurately estimate subtle vessel structures from coronary angiograms. To minimize the ion-

izing radiation exposure of patients and medical personnel, low-power X-ray is used during X-ray coronary angiography, usually leading to noisy and low-contrast coronary angiograms. As a result, it is difficult to distinguish vessels from the background artifacts¹ that share similar appearances with vessel structures.

During X-ray coronary angiogram acquisition, a special cardiac catheter is utilized to inject a contrast agent into the coronary artery. With the contrast agent taking effect, blood vessels gradually emerge, leaving a sequence of coronary angiography images under the X-ray. In such a coronary angiography sequence, the first frame with no contrast agent injected is the *mask frame*. No vessel is shown in the mask frame. On the contrary, the frame with a fully injected contrast agent is known as the *contrast frame*. Note that in this paper, we use the coronary angiogram to indicate the contrast frame in particular. Vessels are shown in coronary angiograms. Our objective is to segment vessels out of the coronary angiograms.

Existing vessel segmentation methods can be classified into four main categories: traditional methods [17, 23], supervised methods [8, 25], domain adaptation methods [3, 31], and unsupervised methods [4, 15]. Traditional methods are typically based on predefined rules that require significant expertise and manual model tuning, leading to limited model expressiveness and generality. Supervised methods require a massive amount of annotated data for training, though public large-scale annotated vessel datasets are practically unavailable. The complex vessel structure consists of numerous tiny branches that easily fade into the image background artifacts, making the manual annotation process extremely laborious and time-consuming, even for professional medical experts. The effectiveness of domain adaptation methods is largely dependent on the quality of annotated source domain dataset and constrained by the gap between the source domain and target domain. Existing unsupervised segmentation methods for natural images, such

¹Note that this paper uses artifacts to represent the factors (e.g., diaphragm, catheter, and bones) making segmentation difficult.

as animals and flowers, can hardly work on medical images due to their thorny characteristics—numerous tiny branches and confusing background artifacts.

Existing self-supervised methods [6, 24] learn useful representations by solving other pretext tasks on large-scale unlabeled data. However, no existing self-supervised methods are designed for segmentation tasks due to the complexity of semantic segmentation. In this paper, we exploit specific characteristics of the coronary angiography sequence and design a novel self-supervised vessel segmentation method.

Specifically, we propose to learn self-supervised vessel representations by simultaneously training two adversarial networks that synthesize fake vessels on mask frames and segment vessels out of coronary angiograms. These learned vessel representations can be applied to multiple vessel segmentation tasks by directly using the pretrained model.

Without labeled vessel segmentation maps, we design a fractal synthetic module for self-supervised learning. Fractals synthesized by the fractal synthetic module are then utilized to guide the generation of vessels and serve as segmentation maps of synthetic fake coronary angiograms. We introduce an attention-guided generator to confirm that vessels of synthetic fake coronary angiograms match input segmentation maps. We also apply the idea of cycle consistency in CycleGAN [39] to segmentation tasks. In our framework, the two adversarial networks for vessel synthesis and segmentation form a cycle to produce reconstructed coronary angiograms and reconstructed segmentation maps. We further utilize segmentation loss to enforce the consistency between segmentation maps and reconstructed segmentation maps.

To support our research and facilitate the work of other researchers, we create an X-ray angiography coronary artery disease (XCAD) dataset. The XCAD dataset contains 1621 mask frames and 1621 coronary angiograms in the training set, and 126 coronary angiograms annotated by experienced radiologists in the testing set. Experimental results on the XCAD dataset demonstrate the effectiveness of the proposed method on coronary vessel segmentation. Moreover, our method shows competitive performance with other retinal vessel segmentation methods on the DRIVE dataset [34] and the STARE dataset [13].

The main contributions of this paper are summarized as follows:

- To our best knowledge, we are the first to design a self-supervised method for vessel segmentation. Our method solves vessel segmentation tasks of both coronary angiograms and retinal images, with self-supervised vessel representations learned from unannotated coronary angiography images.
- We build and release the first X-ray angiography coronary artery disease (XCAD) dataset ².

Traditional vessel segmentation methods [17, 23] require designing predefined rules for specific images. Khan *et al.* [17] designed several filters for retinal image denoising, enhancement and finally for vessel segmentation. Memari *et al.* [23] proposed to firstly enhance retinal images using contrast limited adaptive histogram equalization and several filters. Then they utilized a genetic algorithm enhanced spatial fuzzy c-means method for extracting an initial vessel segmentation map. Finally, the segmentation is further refined by an integrated level set approach.

Traditional methods with manually designed strategies can only be used for specific tasks and have poor scalability, e.g., methods for retinal vessel segmentation cannot solve the coronary vessel segmentation problem. In contrast, our method successfully solves the problems of both retinal vessel segmentation and coronary vessel segmentation. Moreover, our method is scalable and easy to be utilized.

2.2. Supervised Methods for Vessel Segmentation

At the early stage of supervised vessel segmentation, Esfahani *et al.* [25] used Top-Hat transform to enhance the input angiograms. Then, the vessel regions can be recognized by training Convolutional Neural Networks (CNNs) with quantities of patches. Khowaja *et al.* [18] applied bidirectional histogram equalization on the inverted green channel to enhance the retinal images in supervised retinal vessel segmentation. Soomro *et al.* [33] utilized fuzzy logic and image processing tactics for pre-processing, and they removed the noisy pixels for post-processing. These methods require specifically designed pre-processing and post-processing strategies.

Mask images are utilized to distinguish vessels from artifacts and remove the influence of background artifacts. Yang *et al.* [37] utilized the DeepMatching method [30] for the registration between the mask frames and coronary angiograms, then used both of them as multi-channel inputs to provide enhanced information of the vessel structure. The performance of this method highly relies on the registration for paired mask frames and coronary angiograms. On the contrary, our method does not need to use paired mask frames and coronary angiograms.

UNet [32] is mostly used as the backbone of vessel segmentation [8, 33, 36]. Fan *et al.* [8] proposed an octave

²<https://github.com/AISIGSJTU/SSVS>

UNet for accurate retinal vessel segmentation, which adopts octave convolution for multiple-spatial-frequency features learning. Yang *et al.* [36] studied the segmentation of the major vessels in X-ray coronary angiograms with UNet on annotated datasets. Supervised methods require complex vessel annotations. Our method alleviates the vessel annotation burden by self-supervised learning.

2.3. Domain Adaptation Methods

Domain adaptation [1] transfers knowledge from the annotated dataset in the source domain to the unannotated dataset in the target domain. An adversarial network [9] is utilized for domain adaptation in many semantic segmentation tasks [12, 5]. Adversarial training generates domain-invariant features through domain confusion. During this process, cycle consistency is usually employed for preserving structures [11, 38].

In medical image segmentation, Dou *et al.* [7] studied domain adaptation between CT and MRI by proposing a plug-and-play adversarial domain adaptation network to align feature spaces of both domains presenting significant domain shift. A domain adaptation method named MMD [3] was proposed for brain tissue segmentation by minimizing the maximum mean discrepancy between the source domain and target domain. YNet [31] extended classification-based domain adaptation techniques to segmentation networks by regularizing the encoder features.

These methods fail to handle tasks that lack large-scale annotated datasets in a close source domain. However, our method does not require any annotated dataset as the source domain.

2.4. Unsupervised Segmentation Methods

Xu *et al.* [15] proposed a method named Invariant Information Clustering. It can automatically partition the input images into clusters that are recognized as different semantic classes. Another method named ReDO [4] utilized an adversarial architecture to extract the object mask of the input, then redrew a new object at the same location with different textures or colors. Because segmentation objects and backgrounds of medical images are very similar and difficult to distinguish, these methods are less effective on medical image segmentation. In contrast, our method takes into account the characteristics of medical images and outperforms these methods on vessel segmentation of coronary angiograms and retinal images.

2.5. Self-supervised Representation Learning

Self-supervised learning methods construct pretexts to learn representations from large-scale unsupervised data. Spatial representations are learned by predicting the relative positions between two image patches [6, 26]. Similar studies designed pretext tasks for image inpainting [28],

super-resolution [21] and image colorization [20] by applying transformations on original images. Different from single pretext tasks, Ren *et al.* [29] learned more generalizable high-level visual representations from multi-task including depth, surface normal and instance contour. Misra *et al.* [24] employed Siamese networks to input multiple video frames in parallel and learn temporal representations by shuffling image sequences. Xu *et al.* [35] learned both spatial and temporal information by sorting the order of 3D clips. SpeedNet [2] predicted the speed of the video from the input of full video sequences. These learned representations are proved to be helpful to action recognition, image classification, and object detection tasks, by finetuning the pretrained model on annotated datasets. However, it is hard to design a suitable pretext task and learn useful representations for complex semantic segmentation. We propose to use a fractal synthetic module for self-supervised learning. Our method learns representations for vessel segmentation by adversarial vessel synthesis and segmentation.

3. Methodology

3.1. Overview

In this section, we present the details of the proposed method. We generate fake coronary angiograms and vessel segmentation maps at the same time, using unpaired mask frames *mask* and coronary angiograms *realY* as inputs. Figure 1 depicts an illustration of the overall framework.

First of all, a fractal synthetic module synthesizes random fractals *realX* in a designed policy. These synthetic fractals are further utilized to guide the synthesis of fake vessels on mask frames. Then, the attention-guided generator utilizes fractals *realX* and mask frames *mask* as inputs, and generates fake coronary angiograms *fakeY*. After that, fractals can be treated as vessel segmentation maps of corresponding fake coronary angiograms. Finally, the segmentation generator segments vessels out of coronary angiograms and recovers vessel segmentation maps *recX*, which forms a reconstruction cycle as the upper orange area of Figure 1.

Similarly, the coronary angiogram reconstruction cycle is shown in the bottom blue area of Figure 1. For input coronary angiograms *realY*, the segmentation generator produces segmentation maps *fakeX*. These segmentation maps are further input into the attention-guided generator to reconstruct coronary angiograms *recY*.

3.2. Fractal Synthetic Module

Fractals are simple graphic patterns rendered by mathematical formulas. It is demonstrated that fractals can assist in learning image representations for recognizing natural scenes and objects. Kataoka *et al.* assisted natural image understanding by pretraining classification networks on an automatically generated Fractal DataBase [16]. However,

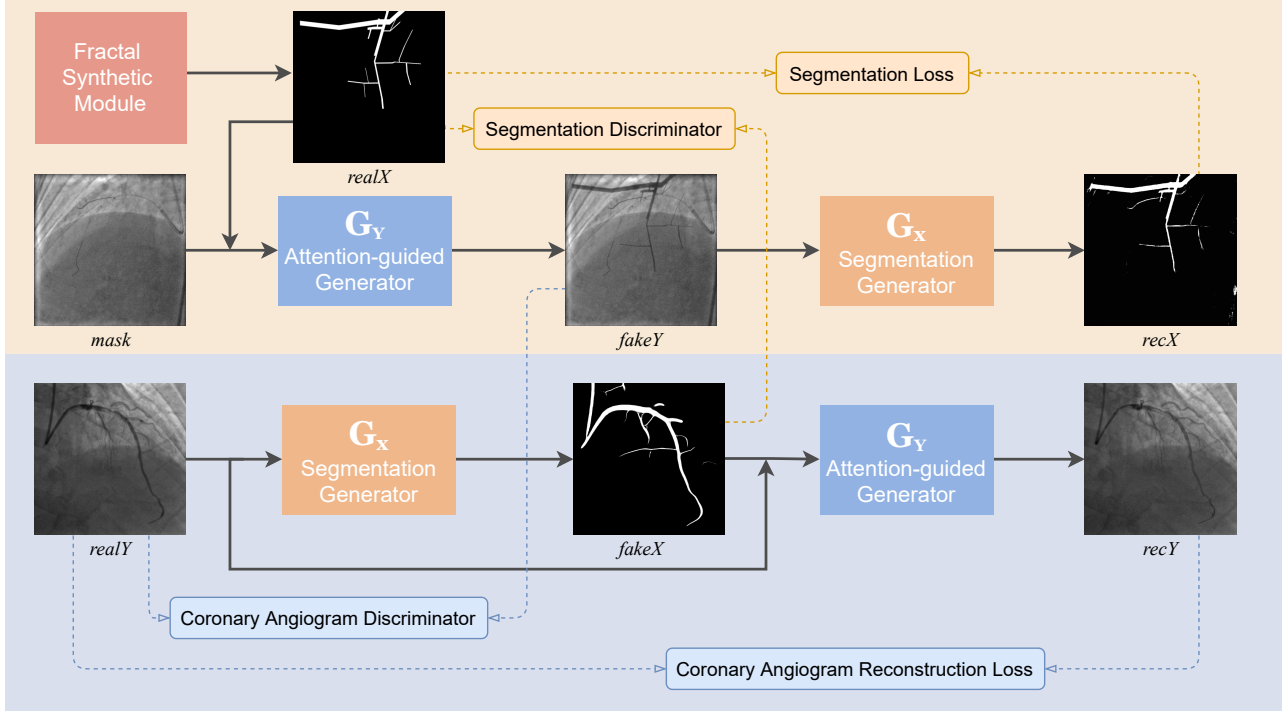


Figure 1. The framework of the proposed method. X indicates the segmentation map and Y indicates the coronary angiogram. Fractal synthetic module synthesizes segmentation maps $realX$ for self-supervised learning. Attention-guided generator generates fake coronary angiograms $fakeY$, while segmentation generator obtains segmentation maps $fakeX$ from input coronary angiograms $realY$. Both generators are applied twice and complete two reconstruction cycles, obtaining reconstructed segmentation maps $recX$ and reconstructed coronary angiograms $recY$. The two reconstruction cycles are shown in the upper orange area and bottom blue area, respectively. Solid lines show data flows, and dashed lines indicate the flow of values to loss functions. *Best viewed in color.*

one limitation of fractals is that the rendered fractal patterns consist of discrete points without textures, which limits the application of fractals. Therefore, we propose to use synthetic fractals as segmentation maps and add realistic textures from the attention-guided generator to these fractals.

Unlike Fractal DataBase that synthesized different fractals by designing a function to literally draw points on a black background, we synthesize fractals that look similar to vessels by literally drawing rectangles on a black background and adding local distortions on it. We design a fractal space as follows:

$$\mathcal{X} = \{(Draw, s_d), (Affine, s_a), (Rotate, s_r)\}, \quad (1)$$

where *Draw* draws random rectangles with branches and s_d controls the depth of the branch. Moreover, *Affine* applies a piecewise affine transformation with a random scale s_a to add local distortions on these rectangles and make them present a curved shape. The piecewise affine transformation places a regular grid of points on the input and randomly moves the neighborhood of these points around via affine transformations. *Rotate* applies rotations with a random angle s_r to make fractals present more various shapes. Due to the space limitation, more details of fractal synthesis are

presented in the supplementary material. We can synthesize any number of random fractals in space \mathcal{X} .

3.3. Attention-guided Generator

The attention-guided generator aims to generate vessels of given fractal shapes on mask frames and transform mask frames to coronary angiograms. The main difference between coronary angiograms and mask frames is the presence and absence of vessels. Thus, the attention-guided generator only generates vessels on specific areas and keeps the rest parts unchanged. Segmentation maps enable some specific areas to get more focus, making the areas of synthetic vessels match focused areas. We utilize the following formulation to restrict the synthetic vessels on specific areas and calculate output coronary angiograms

$$fakeY = realX \odot G(realX) + (1 - realX) \odot mask, \quad (2)$$

where $realX$, $mask$ and $fakeY$ represent segmentation maps, input mask frames, and output coronary angiograms, respectively. \odot represents hadamard product. $G()$ is a generative network for transforming the texture style of segmentation maps to the texture style of vessels. We use $realX \odot G(realX)$ to generate fake vessels with the shape

of segmentation maps $realX$ and the texture of realistic vessels. Then, we merge the vessels to background areas of mask frames $(1 - realX) \odot mask$ and obtain fake coronary angiograms $fakeY$.

The attention-guided generator is applied twice to complete the reconstruction cycle. For segmentation maps $fakeX$, we get reconstructed coronary angiograms $recY$ with a similar formulation as follows:

$$recY = fakeX \odot G(fakeX) + (1 - fakeX) \odot realY. \quad (3)$$

Note that our method does not require paired inputs of mask frames and coronary angiograms. We directly use real coronary angiograms $realY$ as backgrounds and avoid troublesome alignments of mask frames and coronary angiograms.

3.4. Optimization Objective

3.4.1 Adversarial Loss

For each generator, a discriminator is iteratively trained to compete against the generator in the manner of two-player minimax.

The attention-guided generator G_Y tries to generate images that look similar to coronary angiograms, while coronary angiogram discriminator D_Y attempts to distinguish between real and fake coronary angiograms. We use the MSE loss inspired by LSGAN [22] to calculate the adversarial loss. The adversarial loss of generator has the form

$$\begin{aligned} \mathcal{L}_{advG}(G_Y, D_Y, X, Y) \\ = \mathbb{E}_{X \sim p_{data}(X)}[(1 - D_Y(G_Y(X)))^2]. \end{aligned} \quad (4)$$

It aims to improve the plausibility of the output coronary angiograms with the coronary angiogram discriminator, thus fooling the discriminator that the generated $G_Y(X)$ to be real. At the same time, the coronary angiogram discriminator D_Y attempts to distinguish the generated $G_Y(X)$ to be fake and real Y to be real with adversarial loss in the following form

$$\begin{aligned} \mathcal{L}_{advD}(G_Y, D_Y, X, Y) = \mathbb{E}_{X \sim p_{data}(X)}[(D_Y(G_Y(X)))^2] \\ + \mathbb{E}_{Y \sim p_{data}(Y)}[(1 - D_Y(Y))^2]. \end{aligned} \quad (5)$$

Similarly, segmentation generator G_X tries to generate images that look similar to segmentation maps using $\mathcal{L}_{advG}(G_X, D_X, Y, X)$, while segmentation discriminator D_X attempts to distinguish between real and fake segmentation maps with $\mathcal{L}_{advD}(G_X, D_X, Y, X)$.

3.4.2 Cycle Consistency Loss

Adversarial losses alone cannot guarantee that the generator obtains desired outputs. We use cycle consistency to restrict the training without paired inputs.

Coronary Angiogram Reconstruction Loss. The coronary angiogram reconstruction loss \mathcal{L}_{rec} aims to enforce the consistency between reconstructed coronary angiograms $recY$ and input coronary angiograms $realY$. It is expressed as

$$\begin{aligned} \mathcal{L}_{rec}(G_Y, G_X, Y) &= \mathcal{L}_{L1}(recY, realY) \\ &= \mathbb{E}_{Y \sim p_{data}(Y)}[\|G_Y(G_X(Y)) - Y\|_1]. \end{aligned} \quad (6)$$

Segmentation Loss. The segmentation loss \mathcal{L}_{seg} aims to enforce the consistency between reconstructed segmentation maps $recX$ and input segmentation maps $realX$. As a special case of semantic segmentation, coronary vessel segmentation should end up with accurately segmented vessels from coronary angiograms. In other words, it is a binary classification problem for all pixels in coronary angiograms. Hence, the binary cross-entropy loss \mathcal{L}_{BCE} between groundtruth segmentation maps $realX$ and predicted segmentation maps $recX$ is utilized as the segmentation loss, as shown in the following equation

$$\begin{aligned} \mathcal{L}_{seg}(G_X, G_Y, X) &= \mathcal{L}_{BCE}(recX, realX) \\ &= \mathbb{E}_{X \sim p_{data}(X)}[X \log G_X(G_Y(X)) \\ &\quad + (1 - X) \log(1 - G_X(G_Y(X)))] . \end{aligned} \quad (7)$$

3.4.3 Full Optimization Objective

To be concluded, the complete objective loss of the two generators can be formulated as follows:

$$\begin{aligned} \mathcal{L} &= \mathcal{L}_{advG}(G_Y, D_Y, X, Y) + \mathcal{L}_{advG}(G_X, D_X, Y, X) \\ &\quad + \lambda_1 \mathcal{L}_{rec}(G_Y, G_X, Y) + \lambda_2 \mathcal{L}_{seg}(G_X, G_Y, X), \end{aligned} \quad (8)$$

where λ_1 and λ_2 are parameters controlling the relative relation of objective terms.

4. Experiments

4.1. Dataset

XCAD dataset. We build an X-ray angiography coronary artery disease (XCAD) dataset with coronary angiography images obtained during stent placement using a General Electric Innova IGS 520 system. Each image has a resolution of 512×512 pixels with one channel. The training set contains 1621 mask frames and 1621 coronary angiograms. The testing set contains 126 independent coronary angiograms with vessel segmentation maps annotated by experienced radiologists. Note that the training set and the testing set have no shared samples.

Retinal dataset. We further employ two public datasets to validate the effectiveness of the proposed method. The DRIVE dataset [34] consists of 40 color retinal images of size 565×584 pixels. The STARE dataset [13] contains 20

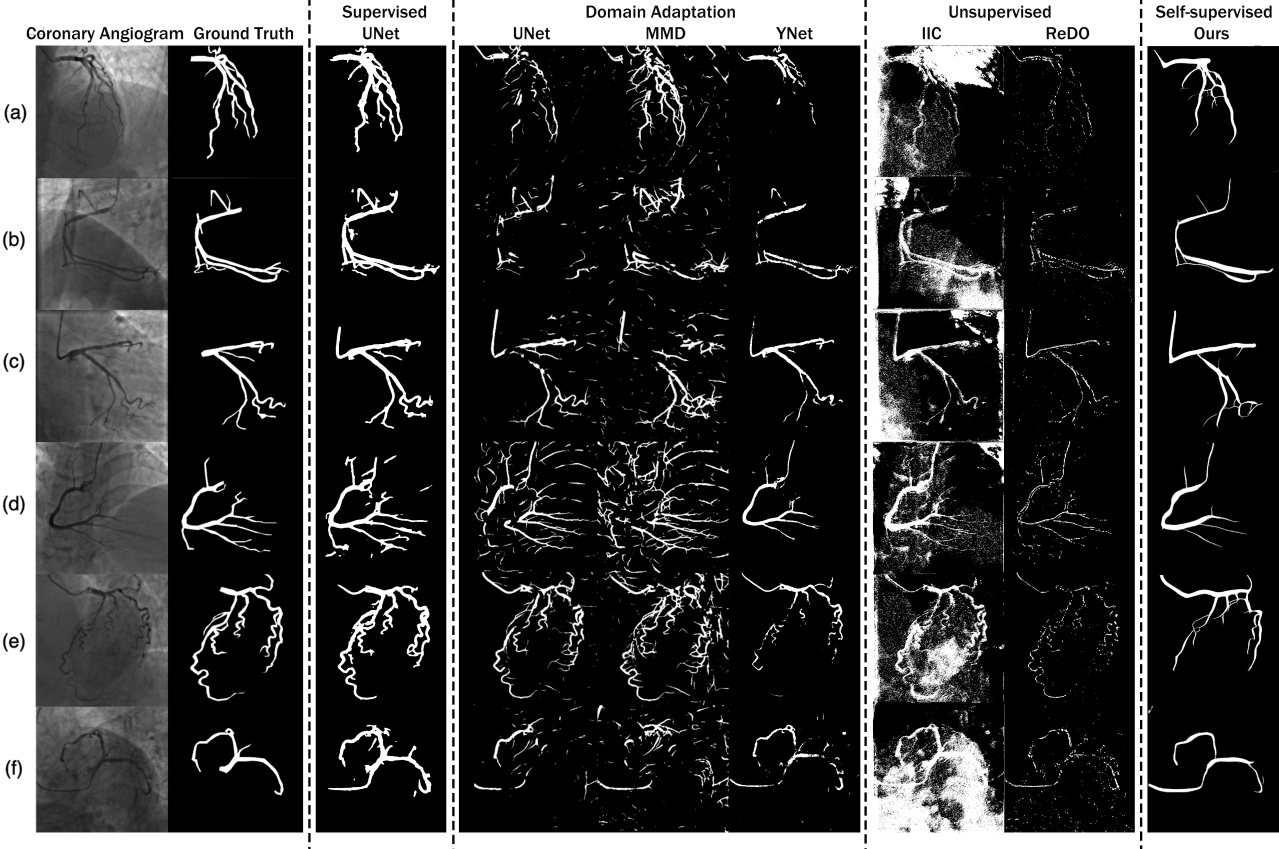


Figure 2. Visualization of coronary vessel segmentation.

color retinal images of size 700×605 pixels. All images have been cropped and then resized to 512×512 pixels.

4.2. Evaluation Metrics

The metrics Jaccard Index, Dice Coefficient, accuracy (Acc.), sensitivity (Sn.) and specificity (Sp.) are used to evaluate the performance of coronary vessel segmentation in different aspects, following the paper [10]. In the DRIVE dataset and the STARE dataset, similar to other retina vessel segmentation methods [8, 33], we use accuracy, sensitivity, specificity and AUC as evaluation metrics.

4.3. Implementation Details

The open-source library PyTorch [27] is employed to implement all the experiments in this paper. The training is done on a 128GB RAM Linux machine with 2 NVIDIA GTX 1080 Ti graphics cards. The Adam optimizer [19] is utilized for the training of the segmentation networks with a batch size of 2. All networks are trained from scratch with a learning rate of 0.0002 for 10 epochs at first. Then, we linearly decay the rate to zero over the next 100 epochs.

The network architecture reuses the existing CycleGAN [39]. The generative network contains 2 downsampling layers, 9 residual blocks and 2 upsampling layers. Besides,

we add an attention layer in the attention-guided generator. The discriminator network is adapted from PatchGAN [14], which contains 4 convolution layers and a final layer for map a 1-dimensional output. Parameters λ_1 and λ_2 in Equation 8 are both set to 10 as in CycleGAN.

4.4. Experimental Results

4.4.1 Coronary Vessel Segmentation

Table 1 reports the performance of vessel segmentation on coronary angiograms with existing methods. The visualization segmentation results are shown in Figure 2.

We firstly compare our method with UNet [32] that is commonly used for supervised vessel segmentation. Considering the small size of the XCAD dataset, we adapt 3-fold cross-validation over the 126 annotated images. Although supervised methods achieve higher performance than our method, supervised methods require a time-consuming and labor-intensive annotation process. However, our method does not require annotation costs and still achieves high performance.

In domain adaptation (DRIVE \rightarrow XCAD), the networks are pretrained on the DRIVE dataset and tested on the XCAD dataset. We use UNet [32] and two state-of-the-

Table 1. Performance comparison of coronary vessel segmentation on the XCAD dataset.

| | Method | Jaccard | Dice | Acc. | Sn. | Sp. |
|------------------------|---------------|-------------------|-------------------|-------------------|-------------------|-------------------|
| Supervised Method | UNet [32] | 0.571 ± 0.009 | 0.724 ± 0.010 | 0.981 ± 0.005 | 0.868 ± 0.011 | 0.996 ± 0.004 |
| | UNet [32] | 0.228 ± 0.020 | 0.365 ± 0.016 | 0.831 ± 0.018 | 0.444 ± 0.020 | 0.906 ± 0.017 |
| Domain Adaptation | MMD [3] | 0.262 ± 0.017 | 0.416 ± 0.021 | 0.873 ± 0.016 | 0.553 ± 0.011 | 0.920 ± 0.013 |
| | YNet [31] | 0.287 ± 0.015 | 0.434 ± 0.019 | 0.891 ± 0.012 | 0.523 ± 0.008 | 0.935 ± 0.014 |
| Unsupervised Method | IIC [15] | 0.124 ± 0.052 | 0.178 ± 0.048 | 0.738 ± 0.107 | 0.487 ± 0.055 | 0.754 ± 0.038 |
| | ReDO [4] | 0.151 ± 0.042 | 0.261 ± 0.037 | 0.753 ± 0.098 | 0.392 ± 0.108 | 0.923 ± 0.018 |
| Self-supervised Method | Ours | 0.389 ± 0.015 | 0.557 ± 0.017 | 0.945 ± 0.009 | 0.583 ± 0.018 | 0.972 ± 0.005 |

Table 2. Ablation Study.

| Method | Jaccard | Dice | Acc. | Sn. | Sp. |
|----------------------------|----------------|--------------|--------------|--------------|--------------|
| Base | 0.229 | 0.363 | 0.850 | 0.320 | 0.877 |
| Base + Attention | 0.305 | 0.464 | 0.902 | 0.487 | 0.931 |
| Base + SegLoss | 0.346 | 0.511 | 0.911 | 0.552 | 0.945 |
| Base + Attention + SegLoss | 0.389 | 0.557 | 0.945 | 0.583 | 0.972 |

art domain adaptation methods MMD [3] and YNet [31] for comparison. Even with knowledge from an annotated source domain, these methods are still inferior to ours. Specifically, more than 35% improvement in Jaccard Index, 28% improvement in Dice Coefficient, 6% improvement in accuracy, 5% improvement in sensitivity, and 4% improvement in specificity are obtained with our method.

Unsupervised methods IIC [15] and ReDO [4] perform poorly on gray-scale X-ray images where the segmentation objects can be hardly distinguished from the background and lack color information. Moreover, the ReDO method is extremely unstable and easy to collapse. Sometimes it fails to segment vessels and outputs all-black segmentation maps. In contrast, our method outperforms these unsupervised methods on all of the five metrics and shows more stable performance. We run all the methods multiple times and provide the variance in Table 1.

4.4.2 Ablation Study

We conduct the ablation study to evaluate the impact of different components and loss functions on the segmentation quality. The results are shown in Table 2. We test the following four setups.

Base. In this setup, we use CycleGAN [39] as the baseline, which deals with the unpaired image-to-image translation of two domains. Specifically, we use synthetic segmentation maps generated by the fractal synthetic module as do-

main X and coronary angiograms as domain Y . Although this baseline can coarsely segment vessels out of coronary angiograms, the segmentation quality is not high and synthetic fake coronary angiograms are very different from real coronary angiograms.

Base + Attention. The attention-guided generator helps the network make use of the self-supervised information in coronary angiograms. Moreover, the segmentation quality improves while the synthetic fake coronary angiograms become more realistic.

Base + SegLoss. Replacing the cycle consistency loss with segmentation loss extensively improves the performance of the vessel segmentation.

Base + Attention + SegLoss. The best performance is obtained when both the attention-guided generator and the segmentation loss are used. Removing the segmentation loss substantially degrades the performance, same as does removing the attention-guided generator. We therefore conclude that attention-guided generator and segmentation loss are all critical to our results.

4.4.3 Cross-domain Verification on Retinal Vessel Segmentation

The proposed self-supervised method can solve different vessel segmentation tasks based on the learned vessel representations from coronary angiography images. In this section, we demonstrate the generality and effectiveness of our

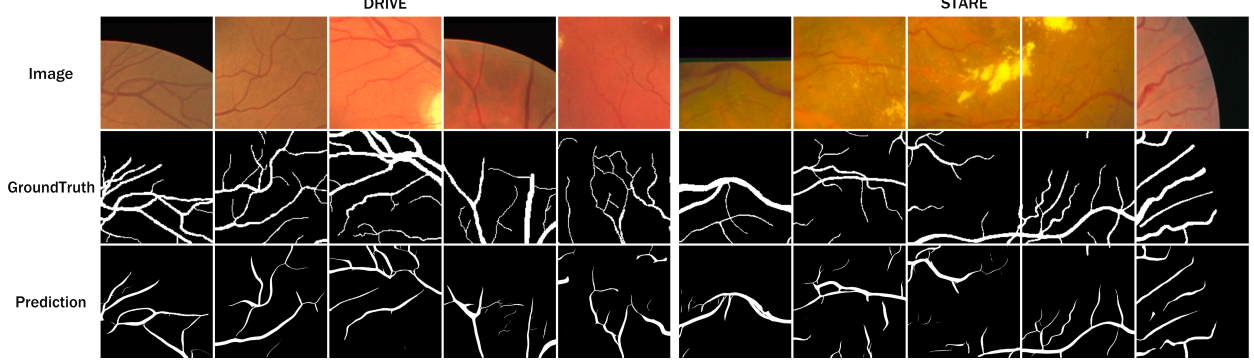


Figure 3. Visualization of retinal vessel segmentation on the DRIVE and STARE datasets.

Table 3. Performance comparison of retinal vessel segmentation on the DRIVE and STARE datasets.

| Method | DRIVE | | | | STARE | | | | |
|------------------------|--------------|-------|-------|-------|-------|-------|-------|-------|-------|
| | Acc. | Sn. | Sp. | AUC | Acc. | Sn. | Sp. | AUC | |
| Traditional Method | Memari [23] | 0.961 | 0.761 | 0.981 | 0.871 | 0.951 | 0.782 | 0.965 | 0.783 |
| | Khan [17] | 0.958 | 0.797 | 0.973 | 0.885 | 0.996 | 0.792 | 0.998 | 0.895 |
| Supervised Method | Khowaja [18] | 0.975 | 0.818 | 0.971 | 0.895 | 0.975 | 0.824 | 0.975 | 0.899 |
| | Fan [8] | 0.966 | 0.796 | 0.982 | 0.889 | 0.974 | 0.816 | 0.987 | 0.901 |
| | Soomro [33] | 0.959 | 0.802 | 0.974 | 0.948 | 0.961 | 0.801 | 0.969 | 0.945 |
| Unsupervised Method | IIC [15] | 0.738 | 0.632 | 0.840 | 0.736 | 0.710 | 0.586 | 0.832 | 0.709 |
| | ReDO [4] | 0.761 | 0.593 | 0.927 | 0.760 | 0.756 | 0.567 | 0.899 | 0.733 |
| Self-supervised Method | Ours | 0.913 | 0.794 | 0.982 | 0.888 | 0.910 | 0.774 | 0.980 | 0.877 |

method on retinal vessel segmentation by directly using the model pretrained on coronary angiography images. Figure 3 shows the visual segmentation results of our method on the DRIVE dataset and the STARE dataset. Table 3 compares our method with the existing methods.

Compared with the traditional methods, the AUC of our method improves by 0.3% on the DRIVE dataset. Although the overall performance of the traditional methods is slightly better than ours, they are specifically designed for retinal vessel segmentation and require complex processing steps. In contrast, our method can solve multiple kinds of vessel segmentation tasks without any annotation or pre-processing. When compared with supervised methods, the performance of the proposed method only decreases by less than 7% on all of the four metrics. Our method surpasses unsupervised methods to a large extent. Quantitatively, our method brings more than 20% improvements in accuracy, 25% improvements in sensitivity, 6% improvements in specificity and 16% improvements in AUC on both datasets.

5. Conclusion

In this paper, we propose a novel self-supervised vessel segmentation method. Different from existing methods, our method applies adversarial learning to learn vessel representations from unannotated coronary angiography images. We further successfully utilize these learned representations in coronary vessel segmentation and retinal vessel segmentation. Extensive experimental results on our proposed XCAD dataset, the DRIVE dataset and the STARE dataset demonstrate the effectiveness of the proposed method.

Acknowledgment

This work is partially funded by National Natural Science Foundation of China (NO. 61872234, 61732010, 61525204), Shanghai Key Laboratory of Scalable Computing and Systems and Intel Corporation. Thanks Shuo Wang for his contribution to data collection.

References

- [1] Shai Ben-David, John Blitzer, Koby Crammer, Alex Kulesza, Fernando Pereira, and Jennifer Wortman Vaughan. A Theory of Learning from Different Domains. *Machine Learning*, 79(1):151–175, 2010. 3
- [2] Sagie Benaim, Ariel Ephrat, Oran Lang, Inbar Mosseri, William T Freeman, Michael Rubinstein, Michal Irani, and Tali Dekel. Speednet: Learning the Speediness in Videos. In *CVPR*, 2020. 3
- [3] Róger Bermúdez-Chacón, Pablo Márquez-Neila, Mathieu Salzmann, and Pascal Fua. A Domain-Adaptive Two-Stream U-Net for Electron Microscopy Image Segmentation. In *ISBI*, 2018. 1, 3, 7
- [4] Mickaël Chen, Thierry Artières, and Ludovic Denoyer. Unsupervised object segmentation by redrawing. In *NeurIPS*, 2019. 1, 3, 7, 8
- [5] Jaehoon Choi, Taekyung Kim, and Changick Kim. Self-Ensembling with GAN-based Data Augmentation for Domain Adaptation in Semantic Segmentation. In *ICCV*, 2019. 3
- [6] Carl Doersch, Abhinav Gupta, and Alexei A Efros. Unsupervised Visual Representation Learning by Context Prediction. In *ICCV*, 2015. 2, 3
- [7] Qi Dou, Cheng Ouyang, Cheng Chen, Hao Chen, and Pheng-Ann Heng. Unsupervised Cross-Modality Domain Adaptation of Convnets for Biomedical Image Segmentations with Adversarial Loss. In *IJCAI*, 2018. 3
- [8] Zhun Fan, Jiajie Mo, Benzhang Qiu, Wenji Li, Guijie Zhu, Chong Li, Jianye Hu, Yibiao Rong, and Xinjian Chen. Accurate Retinal Vessel Segmentation via Octave Convolution Neural Network. *arXiv preprint arXiv:1906.12193*, 2019. 1, 2, 6, 8
- [9] Ian J Goodfellow, Jean Pouget-Abadie, Mehdi Mirza, Bing Xu, David Warde-Farley, Sherjil Ozair, Aaron Courville, and Yoshua Bengio. Generative Adversarial Networks. In *NeurIPS*, 2014. 3
- [10] Mohammad Haft-Javaherian, Martin Villiger, Chris B Schaffer, Nozomi Nishimura, Polina Golland, and Brett E Bouma. A Topological Encoding Convolutional Neural Network for Segmentation of 3D Multiphoton Images of Brain Vasculature Using Persistent Homology. In *CVPR Workshop*, 2020. 6
- [11] Judy Hoffman, Eric Tzeng, Taesung Park, Jun-Yan Zhu, Phillip Isola, Kate Saenko, Alexei Efros, and Trevor Darrell. Cycada: Cycle-Consistent Adversarial Domain Adaptation. In *ICML*, 2018. 3
- [12] Weixiang Hong, Zhenzhen Wang, Ming Yang, and Jun-song Yuan. Conditional Generative Adversarial Network for Structured Domain Adaptation. In *CVPR*, 2018. 3
- [13] AD Hoover, Valentina Kouznetsova, and Michael Goldbaum. Locating Blood Vessels in Retinal Images by Piecewise Threshold Probing of a Matched Filter Response. *IEEE Transactions on Medical Imaging*, 19(3):203–210, 2000. 2, 5
- [14] Phillip Isola, Jun-Yan Zhu, Tinghui Zhou, and Alexei A Efros. Image-to-Image Translation with Conditional Adversarial Networks. In *CVPR*, 2017. 6
- [15] Xu Ji, João F Henriques, and Andrea Vedaldi. Invariant Information Clustering for Unsupervised Image Classification and Segmentation. In *ICCV*, 2019. 1, 3, 7, 8
- [16] Hirokatsu Kataoka, Kazushige Okuyasu, Asato Matsumoto, Eisuke Yamagata, Ryosuke Yamada, Nakamasa Inoue, Akio Nakamura, and Yutaka Satoh. Pre-Training without Natural Images. In *ACCV*, 2020. 3
- [17] Khan Bahadar Khan, Muhammad Shahbaz Siddique, Muhammad Ahmad, and Manuel Mazzara. A Hybrid Unsupervised Approach for Retinal Vessel Segmentation. *BioMed Research International*, 2020, 2020. 1, 2, 8
- [18] Sunder Ali Khwaja, Parus Khwaja, and Imdad Ali Ismaili. A Framework for Retinal Vessel Segmentation from Fundus Images using Hybrid Feature Set and Hierarchical Classification. *Signal, Image and Video Processing*, 13(2):379–387, 2019. 2, 8
- [19] Diederik P Kingma and Jimmy Ba. Adam: A Method for Stochastic Optimization. In *ICLR*, 2015. 6
- [20] Gustav Larsson, Michael Maire, and Gregory Shakhnarovich. Colorization as a Proxy Task for Visual Understanding. In *CVPR*, 2017. 3
- [21] Christian Ledig, Lucas Theis, Ferenc Huszár, Jose Caballero, Andrew Cunningham, Alejandro Acosta, Andrew Aitken, Alykhan Tejani, Johannes Totz, Zehan Wang, et al. Photo-Realistic Single Image Super-Resolution using a Generative Adversarial Network. In *CVPR*, 2017. 3
- [22] Xudong Mao, Qing Li, Haoran Xie, Raymond YK Lau, Zhen Wang, and Stephen Paul Smolley. Least Squares Generative Adversarial Networks. In *ICCV*, 2017. 5
- [23] Nogol Memari, M Iqbal Bin Saripan, Syamsiah Mashohor, Mehrdad Moghbel, et al. Retinal Blood Vessel Segmentation by using Matched Filtering and Fuzzy C-Means Clustering with Integrated Level Set Method for Diabetic Retinopathy Assessment. *Journal of Medical and Biological Engineering*, 39(5):713–731, 2019. 1, 2, 8
- [24] Ishan Misra, C Lawrence Zitnick, and Martial Hebert. Shuffle and Learn: Unsupervised Learning using Temporal Order Verification. In *ECCV*, 2016. 2, 3
- [25] Ebrahim Nasr-Esfahani et al. Vessel extraction in x-ray angiograms using deep learning. In *EMBC*, 2016. 1, 2
- [26] Mehdi Noroozi and Paolo Favaro. Unsupervised Learning of Visual Representations by Solving Jigsaw Puzzles. In *ECCV*, 2016. 3
- [27] Adam Paszke et al. Pytorch: An Imperative Style, High-Performance Deep Learning Library. In *NeurIPS*, 2019. 6
- [28] Deepak Pathak, Philipp Krahenbuhl, Jeff Donahue, Trevor Darrell, and Alexei A Efros. Context Encoders: Feature Learning by Inpainting. In *CVPR*, 2016. 3
- [29] Zhongzheng Ren and Yong Jae Lee. Cross-Domain Self-Supervised Multi-Task Feature Learning using Synthetic Imagery. In *CVPR*, 2018. 3
- [30] Jérôme Revaud, Philippe Weinzaepfel, Zaïd Harchaoui, and Cordelia Schmid. DeepMatching: Hierarchical Deformable Dense Matching. *International Journal of Computer Vision*, 120(3):300–323, 2016. 2
- [31] Joris Roels, Julian Hennies, Yvan Saeys, Wilfried Philips, and Anna Kreshuk. Domain Adaptive Segmentation in Volume Electron Microscopy Imaging. In *ISBI*, 2019. 1, 3, 7

- [32] Olaf Ronneberger, Philipp Fischer, and Thomas Brox. U-Net: Convolutional Networks for Biomedical Image Segmentation. In *MICCAI*, 2015. 2, 6, 7
- [33] Toufique Ahmed Soomro, Ahmed J Afifi, Ahmed Ali Shah, Shafiullah Soomro, Gulsher Ali Baloch, Lihong Zheng, Ming Yin, and Junbin Gao. Impact of Image Enhancement Technique on CNN Model for Retinal Blood Vessels Segmentation. *IEEE Access*, 7:158183–158197, 2019. 2, 6, 8
- [34] Joes Staal, Michael D Abràmoff, Meindert Niemeijer, Max A Viergever, and Bram Van Ginneken. Ridge-based Vessel Segmentation in Color Images of the Retina. *IEEE Transactions on Medical Imaging*, 23(4):501–509, 2004. 2, 5
- [35] Dejing Xu, Jun Xiao, Zhou Zhao, Jian Shao, Di Xie, and Yueling Zhuang. Self-Supervised Spatiotemporal Learning via Video Clip Order Prediction. In *CVPR*, 2019. 3
- [36] Su Yang et al. Deep Learning Segmentation of Major Vessels in X-Ray Coronary Angiography. *Scientific Reports*, 9(1):1–11, 2019. 2, 3
- [37] Siyuan Yang, Jian Yang, Yachen Wang, Qi Yang, Danni Ai, and Yongtian Wang. Automatic Coronary Artery Segmentation in X-ray Angiograms by Multiple Convolutional Neural Networks. In *ICMIP*, 2018. 2
- [38] Yue Zhang, Shun Miao, Tommaso Mansi, and Rui Liao. Task Driven Generative Modeling for Unsupervised Domain Adaptation: Application to X-ray Image Segmentation. In *MICCAI*, 2018. 3
- [39] Jun-Yan Zhu, Taesung Park, Phillip Isola, and Alexei A Efros. Unpaired Image-to-Image Translation using Cycle-Consistent Adversarial Networks. In *ICCV*, 2017. 2, 6, 7